

## Full Length Article

## 3D interconnected honeycomb-like and high rate performance porous carbons from petroleum asphalt for supercapacitors



Lei Pan, Xinxin Li, Yixian Wang, Jialiang Liu, Wei Tian, Hui Ning, Mingbo Wu\*

State Key Laboratory of Heavy Oil Processing, College of Chemical Engineering, China University of Petroleum, Qingdao 266580, People's Republic of China

## ARTICLE INFO

## Article history:

Received 24 November 2017

Revised 6 March 2018

Accepted 16 March 2018

Available online 16 March 2018

## Keywords:

Hierarchical porous carbon

Petroleum asphalt

Molten salt medium

Supercapacitors

## ABSTRACT

In this paper, 3D interconnected honeycomb-like hierarchical porous carbons (HPCs) are prepared from petroleum asphalt via in-situ KOH activation in a molten salt medium. As symmetry two electrodes for supercapacitors, HPCs with high specific surface area of  $2227 \text{ m}^2 \text{ g}^{-1}$  show high rate performance, i.e.  $265 \text{ F g}^{-1}$  at  $0.05 \text{ A g}^{-1}$ ,  $221 \text{ F g}^{-1}$  at  $20 \text{ A g}^{-1}$ , and superior cycle stability with 91.1% capacitance retention at  $5 \text{ A g}^{-1}$  after 10,000 cycles in 6 M KOH electrolyte. This facile strategy to prepare massive HPCs from cheap petroleum asphalt can provide high performance electrode materials for energy storage devices.

© 2018 Elsevier B.V. All rights reserved.

## 1. Introduction

The increasing consumption of fossil fuels has caused serious concerns about the fast depletion of existing fossil fuel reserves and the associated alarming greenhouse gas emissions and pollutions. It is urgent to find renewable environmental friendly energy devices [1,2]. Correspondingly, supercapacitors as a tradition energy storage device, also known as electrochemical double layer capacitors (EDLCs) attract tremendous attention due to its high power density, long cycle life and short charged-discharged time [3–5]. As we know, the electrochemical performance of supercapacitors mainly depends on the electrode material [6]. Carbonaceous materials [7], transition-metal oxides [8–14], conducting polymers are the main electrode materials of energy devices. In the past decades, carbon-based materials have attracted great attention because of their stable chemical properties and better cycle stabilities [15,16]. Various nanostructured carbon material such as carbon nanotubes/nanorods [17–19], carbon dots [20], nanofibers, graphene [7,21], nanosheets [22], nanospheres [23], and nanocages [24–26] have been investigated. However, each type of carbon materials has its own benefits and drawbacks. Carbon nanotubes possess excellent electrical conductivity and have a large ionic accessible surface area which ensuring an outstanding rate performance, however, their specific capacitances are rather limited owing to that the structure of interior tube can't expose the active sites completely. Graphene as a single layer of carbon

atoms has attracted considerable interests because of its large theoretical surface area and excellent electrical conductivity, nevertheless, its specific capacitance is still far below the theoretical value as a result of the irreversible agglomeration. It is well known that 3D hierarchical porous carbon nanostructures not only provide a continuous electron pathway to ensure good electrical contact, but also facilitate ion transport via shorten ion diffusion distance [27,28]. Furthermore, it was reported that the pore size less than 1 nm would lead to anomalous increase in carbon capacitance [29–32], it is urgent to find out new ways for preparing microporous 3D hierarchical porous carbons [33]. Up to now, great efforts have been devoted to preparing porous carbon by template approaches [34–37], during which various soft templates and hard templates have been employed. Unfortunately, most templates can't dissolve in water, thus acid must be used to remove the template, resulting time consuming and pollution. Moreover, the size and morphology of the porous carbon are limited by the template. In a word, the shortcomings of the template mentioned above limit its commercial application [38].

As a byproduct of petroleum refinery, petroleum asphalt has been mostly used for road construction and burned as fuel. Although petroleum asphalt has been reported to prepare carbon materials for water purification [39], gas adsorption, energy storage and conversion [40,41], How to fulfill the high-value utilization of petroleum asphalt with large amount of polycyclic aromatic hydrocarbons is still a big challenge. Tour et al. used the asphalt with KOH activation prepare ultrahigh surface area porous carbon as anode of lithium ion batteries shows high coulomb efficiency, areal capacity and high discharging/charging rate [42]. Song et al.

\* Corresponding author.

E-mail address: [wumb@upc.edu.cn](mailto:wumb@upc.edu.cn) (M. Wu).

used mesophase pitch and nano-CaCO<sub>3</sub> as templates synthesis mesoporous soft carbon as anode of sodium ion batteries indicating its excellent rate capability and cycling performance [43]. All of them demonstrated petroleum asphalt is an excellent raw material in energy storage.

Herein, we designed in-situ KOH activation coupled with molten salt to synthesize 3D interconnected honeycomb-like hierarchical porous carbons for supercapacitors. Molten salt (mole ratio of NaCl to KCl is 0.5/0.5) was used as separator for aromatic domains of petroleum asphalt, which facilitate the sufficient contact between KOH and asphalt, thus microporous carbons with high surface area were obtained. The effects of the calcination temperature and the ratio of molten to asphalt on the electrochemical performance of as-made HPCs were investigated. To our best knowledge, there was no work on metal chlorides as medium combined with KOH activation to prepare electrodes for supercapacitors has been reported.

## 2. Experimental

### 2.1. Preparation of HPCs

Petroleum asphalt was obtained from Sinopec Group (7.1 wt% saturates, 24.9 wt% aromatics, 46.1 wt% resins and 18.0 wt% asphaltenes). The elemental analysis shows that it has 89.33 wt% of carbon, 2.32 wt% of hydrogen, 2.67 wt% of sulfur, and 5.68 wt% of oxygen, sodium chloride and potassium chloride were bought from Aladdin Ltd ( $\geq 99.5\%$ ). KOH was purchased from Sinopharm Ltd ( $\geq 85.0\%$ ). All other chemicals were of analytical grade (AR) and used without any further purification process. 0.5 g petroleum asphalt dissolved in toluene and ultrasonic treated for 10 min, 10 g melt salt (mole ratio of NaCl to KCl is 0.5/0.5) and 1.5 g KOH were firstly grounded in an agate mortar for 20 min, then added to the obtained asphalt solution. The resulting solution was sufficiently stirred and evaporated at 90 °C to remove toluene. Subsequently, the mixture was transferred to a corundum boat in a horizontal tube oven and heated to 800 °C at 5 °C min<sup>-1</sup> and held at 800 °C for 120 min under N<sub>2</sub> atmosphere, then cooled to room temperature and washed with deionized water. Finally, HPCs were obtained after drying in an oven at 60 °C for 24 h. The prepared HPCs were also named as HPC<sub>Z-T</sub>. In order to illustrate the role of KOH, the MS<sub>Z-T</sub> detailed preparation process was similar to HPC<sub>Z-T</sub> without the addition of KOH, where Z and T represent the mass of melt salt to asphalt and carbonization temperature, respectively.

### 2.2. Characterization

The morphology and microstructure of the prepared HPCs were characterized by field emission scanning electron microscopy (SEM, Hitachi S-4800 Japan), Transmission electron microscopy (TEM, JEM-2100UHR, Japan), and X-ray diffraction (XRD X'Pert PRO MPD, Holland). FTIR spectra of powder samples with KBr as the compressed slices were recorded (FT-IR, Nicolet6700). The Raman spectroscopy (Renishaw RM2000) was studied by X-ray photoelectron spectroscopy (XPS, Thermo Scientific Escalab 250XI). Thermogravimetry (TG, Shimadzu TA-60Ws) was recorded on Thermal Analyzer at a heating rate of 10 °C min<sup>-1</sup> in nitrogen from room temperature to 1000 °C. The pore structure was determined by nitrogen adsorption-desorption isotherms on a sorptometer (Micromeritics, ASAP 2020, America), while the BET surface area was obtained by BET (Brunauer-Emmett-Teller) equation, the total pore volume ( $V_t$ ) was obtained under a relative pressure ( $P/P_0$ ) of 0.99. The mesopore size distribution was calculated by using the adsorption branch of the Barrett-Joyner-Halenda (BJH) method, and the micropore size distribution was estimated

by the Horvath-Kawazoe (HK) method. The micropore volume ( $V_{mic}$ ) was obtained by using the t-plot method. The average pore diameter ( $D_{ap}$ ) of HPCs was calculated by the equation of  $D_{ap} = 4V_t/S_{BET}$ .

### 2.3. Preparation and electrochemical measurements of HPCs electrodes

As obtained HPCs have high conductivity, no carbon black was needed to make electrode slurry, which was fabricated by mixing HPCs and polytetrafluoroethylene (PTFE) with a weight ratio of 9:1. Then, the mixture was rolled into thin film and further cut into round films (12 mm in diameter). The each round film with 3 mg cm<sup>-2</sup> of mass loadings were dried in vacuum oven at 120 °C for 2 h, and then pressed onto nickel foams for fabricating supercapacitors electrodes, and finally soaked in 6 M KOH electrolyte under vacuum for 60 min. A button-type supercapacitor was assembled by two similar electrodes and separated by a piece of polypropylene membrane. The cyclic voltammetry (CV) and electrochemical impedance spectroscopy (EIS) measurements were conducted on CHI760E electrochemical workstation (Chenhua, Shanghai, China). The galvanostatic charge-discharge (GCD) measurements and cycle life tests were conducted on a supercapacitance test system (SCTs, Arbin Instruments, USA). The specific capacitance of the working electrodes was calculated from the galvanostatic discharge process via the following equation:

$$C = \frac{4I}{m \frac{\Delta V}{\Delta t}} \quad (1)$$

where  $I$  (A) stands for the discharge current,  $m$  (g) represents for the total mass of the active material in two-electrode cell,  $\Delta V$  (V) and  $\Delta t$  (s) are the discharge voltage and the discharge time in the discharge process.

The energy density ( $E$ , Wh kg<sup>-1</sup>) and average power density ( $P$ , W kg<sup>-1</sup>) of the supercapacitors were calculated based on the following equations:

$$E = \frac{1}{2 \times 4 \times 3.6} CV^2 \quad (2)$$

$$P = \frac{E}{\Delta t} \quad (3)$$

where  $V$  (V) represents the working voltage (excluding  $IR$  drop), and  $t$  (h) stands for the discharge time.

## 3. Results and discussion

Fig. 1 illustrates the formation process of the HPCs. The mixture of asphalt KOH and salt was calcination under N<sub>2</sub> atmosphere at heating rate of 5 °C min<sup>-1</sup>, the asphalt melts as the temperature rises up to around 200 °C while the salt still keeps solid state (see Fig. S2a in Supplementary materials), which makes sure the salt and KOH can be wrapped by asphalt. As the temperature increases, light constituent of petroleum asphalt volatilize, polycyclic aromatic hydrocarbons gradually polymerize, the salt melts and form a liquid media when heated up to 657 °C. The crystallization of molten salts pushed carbon out, therefore, carbon product and molten salts showed two separated phases. Meanwhile, hold this temperature for 2 h and the asphalt is activated by wrapped KOH under high temperature [44,45], forming honeycomb-like macropores after the salt removal. In this process, Many micropores can be formed across the walls due to KOH activation [46].

The comparative tests are investigated to evaluate the effect of the calcination temperature to the pore structure of as-made HPCs. Fig. 2a and b show the SEM images of HPC<sub>20-800</sub>, which are composed of numerous interconnected and honeycomb-like porous carbons. The interconnected 3D porous carbon nanostructures

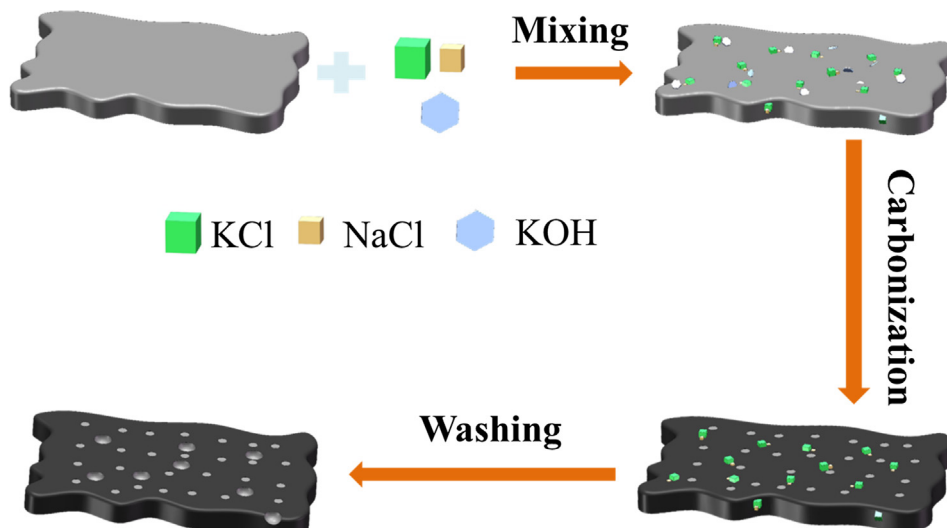


Fig. 1. Preparation schematic of HPCs.

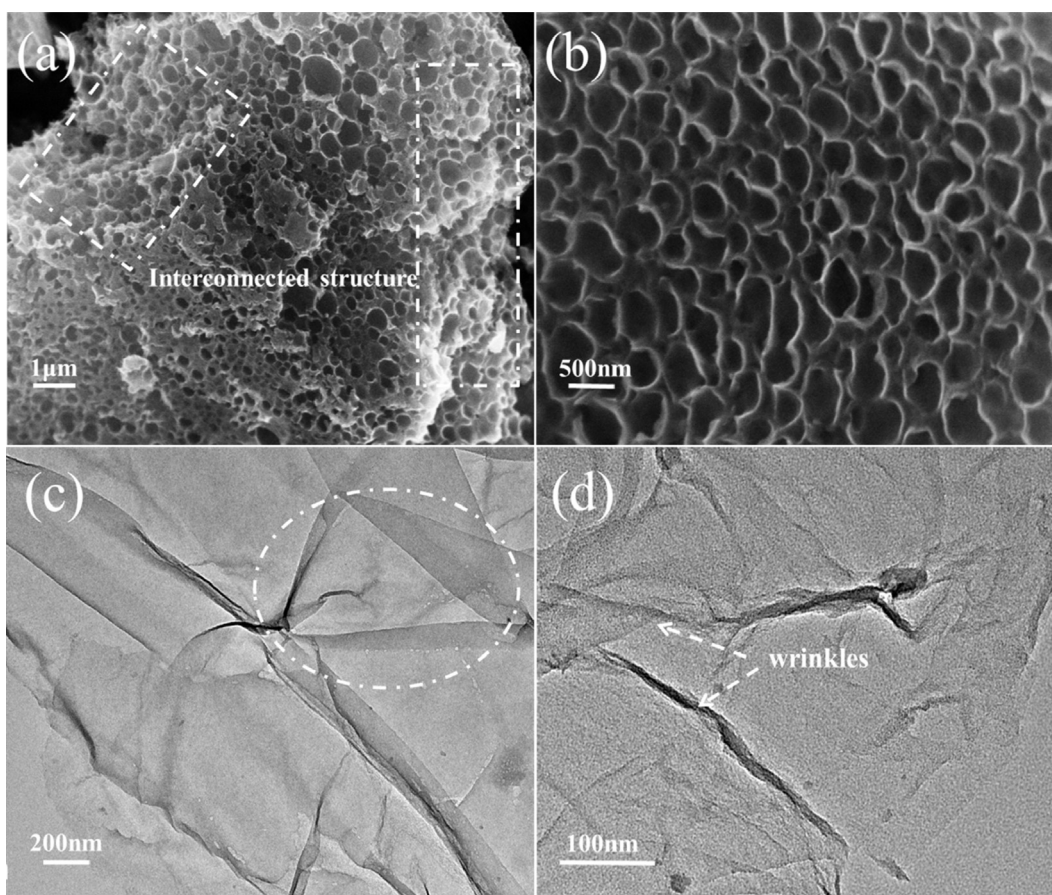
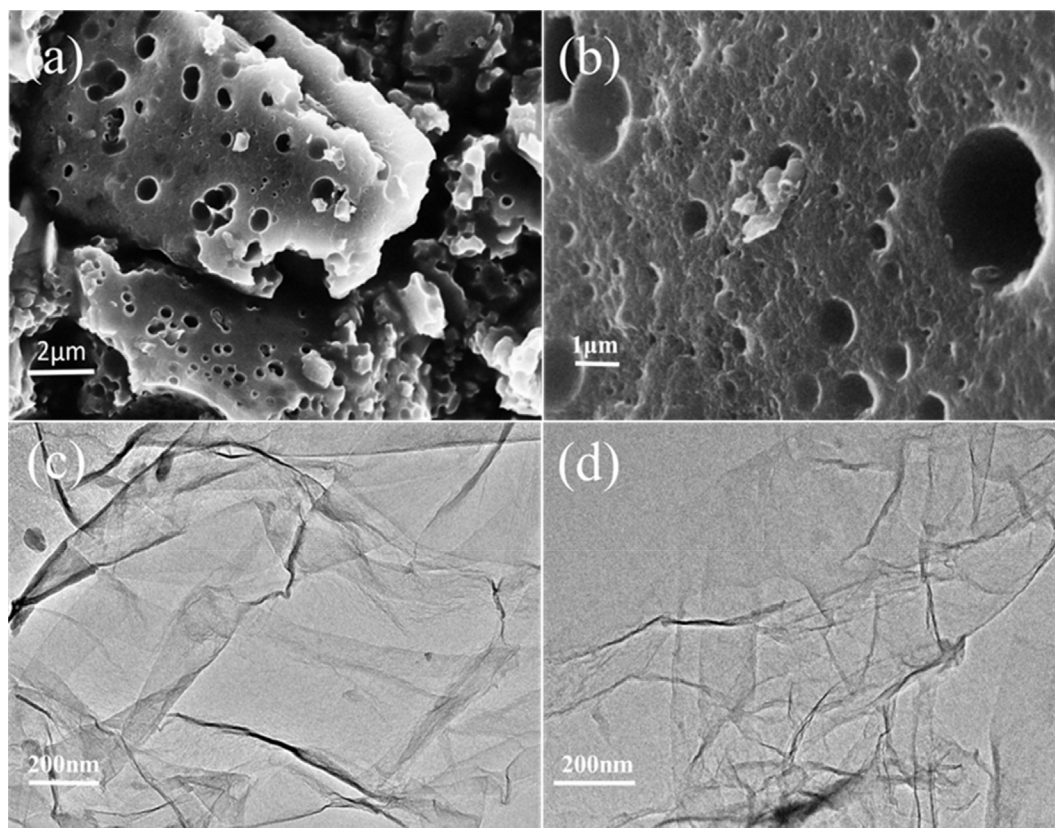


Fig. 2. (a) SEM images of HPC<sub>20-800</sub>, (b), FESEM of HPC<sub>20-800</sub>, (c) and (d) TEM image of HPC<sub>20-800</sub>.

not only provide a continuous electron pathway to ensure good electrical conductivity, but also facilitate ionic transport by shortening diffusion pathways. Fig. 3a shows that the HPCs activated at 700 °C is underdeveloped activation, due to the  $K_2CO_3$  formation from carbon with KOH uncompleted decomposition. As the temperature increases to 900 °C, lots of micropores are damaged by over activated, forming macropores (see Fig. 3b). More detailed morphologies of HPCs can be found in TEM image. The sheet-like

nanostructure of HPC<sub>20-800</sub> can be observed clearly in the TEM image in Fig. 2c and d. The curved structure and nearly transparent to electron beams due to their ultrathin nature. Different from the HPC<sub>20-700</sub> and HPC<sub>20-900</sub> (Fig. 3c and d), the mesopores can be clearly seen in broken HPC<sub>20-800</sub> (highlighted by a white circle in Fig. 2c). The interconnected pores and the wrinkle sheet structures serve as ion-buffering region, which is believed to favor the fast transport of electrolyte ions, result the high rate performance of



**Fig. 3.** (a) SEM image of the HPC<sub>20-700</sub> (b) SEM image of the HPC<sub>20-900</sub> (c) TEM image of the HPC<sub>20-700</sub> (d) TEM image of the HPC<sub>20-900</sub>.

HPCs. To further demonstrate the crystallization of HPCs, Fig. S4c reveals the SAED of HPC<sub>20-800</sub>, suggesting the mainly amorphous structure.

The N<sub>2</sub> adsorption-desorption isotherms are shown in Fig. 4a. The isotherm of HPC<sub>20-800</sub> with high N<sub>2</sub> adsorption at low relative pressure ( $P/P_0 < 0.01$ ) corresponds to the filling of abundant micropores. The isotherms belong to type IV feature with type H<sub>3</sub> hysteresis in the range of 0.4–1.0, indicating the HPCs existence hierarchical pore structure. Hierarchical porous structure can improve the electrochemical performance [22]. Generally, the macropores act as ion-buffering region to minimize the diffusion distances, while the mesopores and micropores provide a large number of accessible surface areas for charge storage. The high  $S_{\text{BET}}$  of HPCs is in favor of enhancing the capacitance of supercapacitors electrode by providing abundant active sites for the adsorption of electrolyte ions. The  $S_{\text{BET}}$  and  $V_{\text{t}}$  of HPC<sub>20-800</sub> are higher, which are 2102 m<sup>2</sup> g<sup>-1</sup> and 0.97 cm<sup>3</sup> g<sup>-1</sup>, respectively. The high surface area of obtained HPCs can be ascribed to its ample pores and its 3D interconnected porous network, which can effectively prevent the agglomeration of graphene-like layers. It is noted that the  $S_{\text{BET}}$  of HPC<sub>20-900</sub> is even larger than that of HPC<sub>20-800</sub> (see Table 1), this small increase ascribes to the mesopores formed from the collapse of micropores due to the over activation by KOH, which can also be seen from their pore size distribution in Fig. 4b. It was easily found out that the pore structure of HPCs can be effectively tuned by alter the heat treatment temperature. Additionally, the ratio of micropore volume to total pore volume of HPC<sub>20-800</sub> reaches as high as 92%, it is believed that the high surface area together with high micropore content endowed HPC<sub>20-800</sub> excellent capacitance performance [31,47]. To explain the function of KOH, the electrochemical performance of MS<sub>20-800</sub> was conducted and the capacitance performances at different current densities was show in Fig. S3a, the barren capacitance was due to undeveloped pore structure

and lower specific surface area (only 10.8 m<sup>2</sup> g<sup>-1</sup>, Fig. S3b supplementary materials).

The surface functional groups are very important to the electrochemical performance [48,49]. So the FT-IR spectra were also recorded in Fig. S1, the Asp means petroleum asphalt raw materials, the FI-IR of HPCs shows absorption bands at 1396 cm<sup>-1</sup>, 1574 cm<sup>-1</sup>, 2924 cm<sup>-1</sup>, 3390 cm<sup>-1</sup> which are ascribed to C–O, C=C, C–H, O–H stretching vibrations respectively. To further detect the surface feature, the Fig. 4c shows the XPS result of HPCs. Similar to the XRD data, no impurities are observed the XPS spectra of HPCs, indicating the complete removal of molten salt and KOH via washing. The high-resolution O1s spectra of HPC<sub>20-800</sub> (525–545 eV) are presented in Fig. 4d. Three fitted peaks correspond to C=O (531.9 eV), O–H (534.0 eV) and C–O (533.4 eV) [50–52], respectively. These functional groups are able to enhance the wettability of HPC<sub>20-800</sub> in aqueous electrolytes [38]. XPS result validates the low oxygen content of HPCs (see Table 2), which indicates the minimal pseudocapacitance on the surface of the electrode. After carbonation process, the oxygen content of the HPCs is less than petroleum asphalt and decreased with the calcination temperature. Fig. 4e displays the Raman spectra of HPCs, D-band at ~ 1320 cm<sup>-1</sup> and G-band at ~ 1590 cm<sup>-1</sup> are displayed. The intense D-band is ascribed to the partial defects owing to abundant pores generated from the KOH activation. Here,  $I_{\text{D}}/I_{\text{G}}$  stands for the defect extent of the HPCs, and the values are 0.84 0.86 and 0.93 respectively, which increase with temperature because the defects generated from the KOH activation. The XRD patterns of HPCs are also given in Fig. 4f, two weak and broad peaks at 23.4° and 43.5° correspond to the 002 and 101 planes of graphite, revealing the amorphous characteristics usually given by KOH activation. To further demonstrate the amorphous structure, the (002) peak of HPC<sub>20-800</sub> is weaker and broader than others, suggesting its more disordered structure [53]. The hazy dispersing

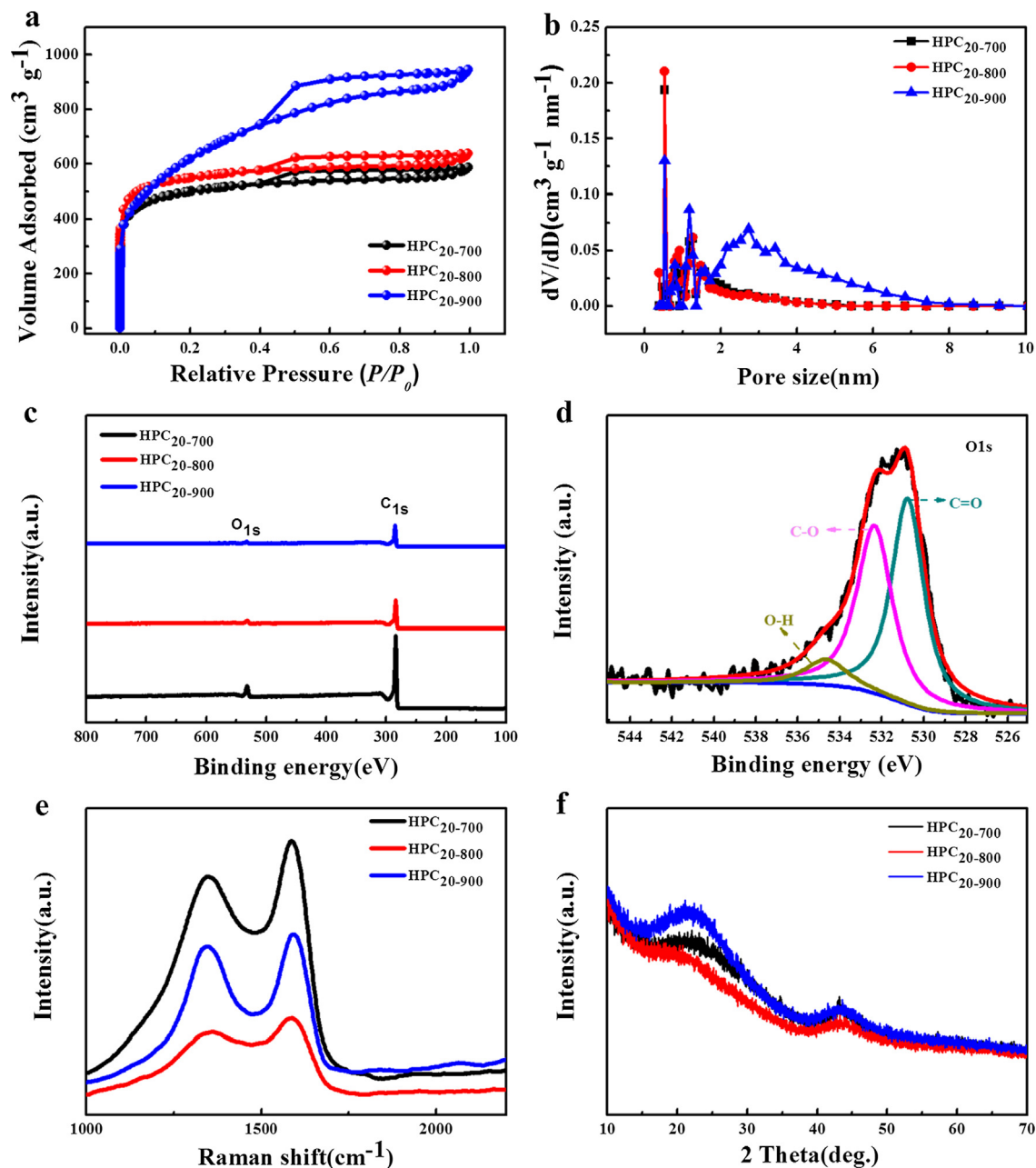


**Fig. 4.** (a)  $N_2$  adsorption–desorption isotherms of HPCs (b) Pore size distributions of HPCs (c) Full XPS spectra of HPCs (d) O1s spectrum of HPC<sub>20-800</sub> (e) Raman spectra of HPCs (f) XRD spectra of HPCs.

**Table 1**

The pore structure parameters of HPCs.

Samples	$D_{ap}$ nm	$S_{BET}$ $m^2 g^{-1}$	$S_{mic}$ $m^2 g^{-1}$	$V_t$ $cm^3 g^{-1}$	$V_{mic}$ $cm^3 g^{-1}$	$V_{mic}/V_t$ %
HPC <sub>20-700</sub>	1.90	1869	1793	0.89	0.81	91
HPC <sub>20-800</sub>	1.83	2102	2055	0.97	0.89	92
HPC <sub>20-900</sub>	2.56	2227	1741	1.43	1.11	78

**Table 2**

Contents of carbon and oxygen elements in HPCs.

Samples	C1s (%)	O1s (%)	O1s		
			C=O (%)	C–O (%)	O–H (%)
HPC <sub>20-700</sub>	96.15	3.85	1.02	1.58	1.25
HPC <sub>20-800</sub>	97.46	2.54	1.34	0.89	0.31
HPC <sub>20-900</sub>	98.44	1.56	1.23	0.30	0.03

diffraction ring in selected area electron diffraction (SAED) patterns verify the amorphous structure of HPC<sub>20-800</sub> (Fig. S4c, Supplementary materials), which is corresponding to its Raman result.

The prepared HPCs were used as electrode material of supercapacitors and their performance was tested in 6 M KOH electrolyte through two-electrode system. As shown in Fig. 5a, the gravimetric capacitance of HPC<sub>20-800</sub> reaches 264, 221 F g<sup>-1</sup> at 0.05 and 20 A g<sup>-1</sup> respectively. In comparison with the capacitance performance shown in Fig. 5a, Fig. S6 shows the galvanostatic charge-discharge curves at different current densities. All the curves exhibit regular isosceles triangle, which demonstrates the HPCs belong to double layer capacitor. It should be noted that the specific capacitance of HPC<sub>20-800</sub> surpasses those reported in most literatures [24,33,45,54–58] (see Fig. 5b). Moreover, the rate performance can reach up to 83.7%, which was high than most literatures. Since

3D interconnected honeycomb-like hierarchical porous carbons nanostructures can serve as ion-buffering region at the charge-discharge process. The CV curves of HPC<sub>20-800</sub> under different scan rates are given in Fig. 5c, HPC<sub>20-800</sub> has the highest capacitance at the scan rate of 2 mV s<sup>-1</sup>. The CV curves can still remain the nearly symmetric rectangular shapes even at the scan rate of 200 mV s<sup>-1</sup>. All the curves exhibit approximately rectangular shapes without distinct redox peaks, demonstrating the ideal electrical double-layer capacitance behavior due to the reversible adsorption and desorption of the electrolyte ions. In addition to the CV test, the GCD test was also employed to analyze the capacitive behavior of HPCs electrodes. HPC<sub>20-800</sub> reveals regular triangle with little IR drop of 0.009 V at 1.2 A g<sup>-1</sup> (see Fig. 5d). As we all know that the CV loop area represents the capacitance of electrode, we can clearly find that HPC<sub>20-800</sub> possesses the best rectangular shapes

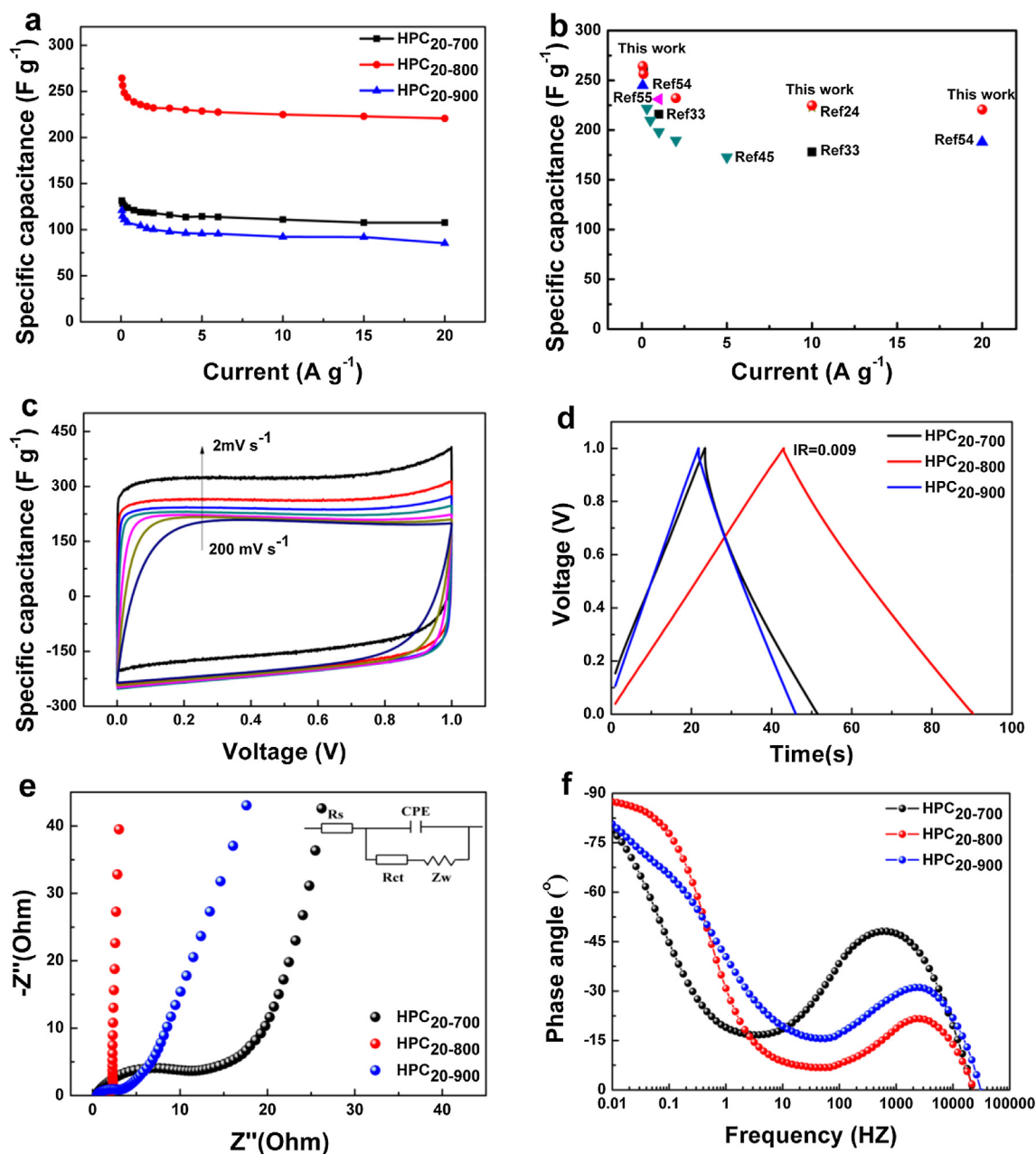


**Fig. 5.** (a) Capacitance of HPCs at different currents density (b) CV curves of HPC<sub>20-800</sub> under 2, 5, 10, 20, 50, 100, and 200 mV s<sup>-1</sup> (c) GCD of HPCs at 1.2 A g<sup>-1</sup> (d) Comparison of specific capacitance HPC<sub>20-800</sub> electrode with other electrodes in two-electrode system (e) Nyquist plots of HPCs (inset was the equivalent circuit model) (f) Bode plots of HPCs.

and the largest area at the same scan rates (as seen in Fig. S2d Supplementary Materials).

To demonstrate the cyclic stability of HPCs, Fig. S2e (Supplementary Materials) shows superior cyclic stability of HPC<sub>20-800</sub> electrode. The capacitance of HPC<sub>20-800</sub> electrode retains 91.1% after 10,000 cycles at 5 A g<sup>-1</sup>. The cyclic stability of HPC<sub>20-800</sub> was high than HPC<sub>20-800</sub> and HPC<sub>20-900</sub>, which was due to the reason that HPC<sub>20-800</sub> has the well-developed interconnected pore structure and lesser pseudocapacitance. The morphologies of HPC<sub>20-800</sub> after life cycle were conducted. Fig. S4a shows that the 3D interconnected honeycomb-like structure was almost unchanged during long life cycle, more detailed morphologies of HPCs can be found in TEM image. Fig. S4b reveals the ultrathin sheet-like structure and crimp structure were served as ion-buffering region, which is believed to favor the fast transport of electrolyte ions, result in high rate performance of HPCs. The energy density of HPC<sub>20-800</sub> supercapacitors reaches 9.16 Wh kg<sup>-1</sup> at 0.05 A g<sup>-1</sup> and remains 5.41 Wh kg<sup>-1</sup> even the current increase to 20 A g<sup>-1</sup> (see Fig. S2f Supplementary Materials). To estimate the capacitive behavior of HPC<sub>20-800</sub>, the Nyquist plot was used to further analyze the ion diffusion and charge transfer resistance of the samples in 6 M KOH electrolyte (Fig. 5e). To quantitatively evaluate the electrode resistance, equivalent circuit model (inset of Fig. 5e) was set up to fit the impedance, the R<sub>s</sub> and R<sub>ct</sub> show smaller value with about 0.58 and 0.78 ohm, respectively, which demonstrates that the interconnected honeycomb-like hierarchical porous carbons structures are favorable both for electron conduction and fast ion transport. To further investigate the capacitance performance of electrode material, the Bode plot was also referred to explain the electrochemical performance. As shown in Fig. 5d, HPC<sub>20-800</sub> electrode presents phase angle (−88°), such a small deviation to the ideal supercapacitors (−90°) can be explained by the thin interconnected honeycomb-like structure, which can serve not only as repository for electrolyte ions, but also as hierarchical pores, facilitating rapid ion transport during the charge-discharge processes.

Besides the activation temperature, the ratio of melt salt to asphalt was also investigated and its effect on the electrochemical performance of final HPCs was also explored (see Fig. S7 Supplementary material). It was easily found that HPC<sub>20-800</sub> exhibits the best electrochemical performance.

#### 4. Conclusions

In summary, a facile and effective strategy was proposed to prepare interconnected honeycomb-like porous carbons for supercapacitors. Metal chlorides salts and KOH were used as separator and dispersive agent for aromatic domains of asphalt and active agent to create pores. This special interconnected honeycomb-like porous structure of HPCs provides the highway both for electronic and ionic transfer, and HPCs display high specific capacitance up to 264 F g<sup>-1</sup> at 0.05 A g<sup>-1</sup> in 6 M KOH electrolyte, with 83.7% rate performance of 221 F g<sup>-1</sup> at 20 A g<sup>-1</sup> and super cycle stability with 91.1% capacitance retention at 5 A g<sup>-1</sup> after 10,000 cycles. In addition to providing promising electrode materials for supercapacitors, this facile strategy also can make electrode with high performance for other energy storage devices.

#### Acknowledgments

This work was supported by the National Natural Science Foundation of China (Nos. 51372277, 51572296, U1662113); The Fundamental Research Funds for the Central Universities (15CX08005A); the Fundamental Research Fund for the Central Universities (No. 14CX02127A)

#### Appendix A. Supplementary material

Supplementary data associated with this article can be found, in the online version, at <https://doi.org/10.1016/j.apsusc.2018.03.122>.

#### References

- [1] Z. Wang, P. Tammela, M. Strømme, L. Nyholm, Cellulose-based supercapacitors: material and performance considerations, *Adv. Energy Mater.* 7 (2017) 1700130.
- [2] G. Gao, H.B. Wu, S. Ding, L.M. Liu, X.W. Lou, Hierarchical NiCo<sub>2</sub>O<sub>4</sub> nanosheets grown on Ni nanofoam as high-performance electrodes for supercapacitors, *Small* 11 (2015) 804–808.
- [3] Z. Wu, L. Li, J.-M. Yan, X.-B. Zhang, Materials design and system construction for conventional and new-concept supercapacitors, *Adv. Sci.* 4 (2017) 1600382.
- [4] J. Yan, Q. Wang, T. Wei, Z. Fan, Recent advances in design and fabrication of electrochemical supercapacitors with high energy densities, *Adv. Energy Mater.* 4 (2014) 1300816.
- [5] J. Liu, L. Zhang, H.B. Wu, J. Lin, Z. Shen, X.W. Lou, High-performance flexible asymmetric supercapacitors based on a new graphene foam/carbon nanotube hybrid film, *Energy Environ. Sci.* 7 (2014) 3709–3719.
- [6] G. Wang, L. Zhang, J. Zhang, A review of electrode materials for electrochemical supercapacitors, *Chem. Soc. Rev.* 41 (2012) 797–828.
- [7] H. Wang, K. Sun, F. Tao, D.J. Stacchiola, Y.H. Hu, 3D honeycomb-like structured graphene and its high efficiency as a counter-electrode catalyst for dye-sensitized solar cells, *Angew. Chem.* 52 (2013) 9210–9214.
- [8] S. Zheng, H. Xue, H. Pang, Supercapacitors based on metal coordination materials, *Coord. Chem. Rev.* (2017), <https://doi.org/10.1016/j.ccr.2017.07.002>.
- [9] Y. Yan, T. Wang, X. Li, H. Pang, H. Xue, Noble metal-based materials in high-performance supercapacitors, *Inorg. Chem. Front.* 4 (2017) 33–51.
- [10] Y. Yan, B. Li, W. Guo, H. Pang, H. Xue, Vanadium based materials as electrode materials for high performance supercapacitors, *J. Power Sources* 329 (2016) 148–169.
- [11] Y. Yan, P. Gu, S. Zheng, M. Zheng, H. Pang, H. Xue, Facile synthesis of an accordion-like Ni-MOF superstructure for high-performance flexible supercapacitors, *J. Mater. Chem. A* 4 (2016) 19078–19085.
- [12] Q.Y. Shan, B. Guan, S.J. Zhu, H.J. Zhang, Y.X. Zhang, Facile synthesis of carbon-doped graphitic C<sub>3</sub>N<sub>4</sub>@MnO<sub>2</sub> with enhanced electrochemical performance, *RSC Adv.* 6 (2016) 83209–83216.
- [13] H. Pang, X. Li, Q. Zhao, H. Xue, W.-Y. Lai, Z. Hu, W. Huang, One-pot synthesis of heterogeneous Co<sub>3</sub>O<sub>4</sub>-nanocube/Co(OH)<sub>2</sub>-nanosheet hybrids for high performance flexible asymmetric all-solid-state supercapacitors, *Nano Energy* 35 (2017) 138–145.
- [14] X. Li, S. Ding, X. Xiao, J. Shao, J. Wei, H. Pang, Y. Yu, N. S co-doped 3D mesoporous carbon-C<sub>6</sub>S<sub>2</sub>O<sub>5</sub>(OH)<sub>4</sub> architectures for high-performance flexible pseudo-solid-state supercapacitors, *J. Mater. Chem. A* 5 (2017) 12774–12781.
- [15] X. Chen, R. Paul, L. Dai, Carbon-based supercapacitors for efficient energy storage, *Nat. Sci. Rev.* (2017) 1.
- [16] W. Yang, W. Yang, F. Ding, L. Sang, Z. Ma, G. Shao, Template-free synthesis of ultrathin porous carbon shell with excellent conductivity for high-rate supercapacitors, *Carbon* 111 (2017) 419–427.
- [17] M. Inagaki, Y. Yang, F. Kang, Carbon nanofibers prepared via electrospinning, *Adv. Mater.* 24 (2012) 2547–2566.
- [18] M. Beidaghi, C. Wang, Micro-supercapacitors based on interdigital electrodes of reduced graphene oxide and carbon nanotube composites with ultrahigh power handling performance, *Adv. Funct. Mater.* 22 (2012) 4501–4510.
- [19] Y. Zhang, J. Wu, T. Xu, Zheng, Y. Xin, Zhang, H. Liu, Binder-free supercapacitive of ultrathin Co(OH)<sub>2</sub> nanosheets-decorated nitrogen-doped carbon nanotubes core-shell nanostructures, *Mater. Technol.* 31 (2016) 521–525.
- [20] X. Miao, X. Yan, D. Qu, D. Li, F.F. Tao, Z. Sun, Red emissive sulfur, nitrogen codoped carbon dots and their application in ion detection and theranostics, *ACS Appl. Mater. Interfaces* 9 (2017) 18549–18556.
- [21] S. Zhu, W. Cen, L. Hao, J. Ma, L. Yu, H. Zheng, Y. Zhang, Flower-like MnO<sub>2</sub> decorated activated multi-hole carbon as high performance asymmetric supercapacitor electrodes, *Mater. Lett.* 135 (2014) 11–14.
- [22] Y.S. Yun, M.H. Park, S.J. Hong, M.E. Lee, Y.W. Park, H.J. Jin, Hierarchically porous carbon nanosheets from waste coffee grounds for supercapacitors, *ACS Appl. Mater. Interfaces* 7 (2015) 3684–3690.
- [23] C.X. Guo, C.M. Li, Construction of one-dimensional nanostructures on graphene for efficient energy conversion and storage, *Energy Environ. Sci.* 4 (2011) 4504–4507.
- [24] K. Xie, X. Qin, X. Wang, Y. Wang, H. Tao, Q. Wu, L. Yang, Z. Hu, Carbon nanocages as supercapacitor electrode materials, *Adv. Mater.* 24 (2012) 347–352.
- [25] Z. Lyu, D. Xu, L. Yang, R. Che, R. Feng, J. Zhao, Y. Li, Q. Wu, X. Wang, Z. Hu, Hierarchical carbon nanocages confining high-loading sulfur for high-rate lithium-sulfur batteries, *Nano Energy* 12 (2015) 657–665.
- [26] Y. Wang, L. Zhang, Y. Wu, Y. Zhong, Y. Hu, X.W. Lou, Carbon-coated Fe<sub>3</sub>O<sub>4</sub> microspheres with a porous multideck-cage structure for highly reversible lithium storage, *Chem. Commun.* 51 (2015) 6921–6924.
- [27] X.-Y. Yang, L.-H. Chen, Y. Li, J.C. Rooke, C. Sanchez, B.-L. Su, Hierarchically porous materials: synthesis strategies and structure design, *Chem. Soc. Rev.* 46 (2017) 481–558.
- [28] X.-L. Su, L. Fu, M.-Y. Cheng, J.-H. Yang, X.-X. Guan, X.-C. Zheng, 3D nitrogen-doped graphene aerogel nanomesh: Facile synthesis and electrochemical

- properties as the electrode materials for supercapacitors, *Appl. Surf. Sci.* 426 (2017) 924–932.
- [29] R. Lin, P.L. Taberna, J. Chmiola, D. Guay, Y. Gogotsi, P. Simon, Microelectrode study of pore size, ion size, and solvent effects on the charge/discharge behavior of microporous carbons for electrical double-layer capacitors, *J. Electrochem. Soc.* 156 (2009) A7.
- [30] H. Zhang, G. Cao, Y. Yang, Z. Gu, Electrochemical capacitive properties of carbon nanotube arrays directly grown on glassy carbon and tantalum foils, *Carbon* 46 (2008) 30–34.
- [31] B. Xu, S. Hou, H. Duan, G. Cao, M. Chu, Y. Yang, Ultramicroporous carbon as electrode material for supercapacitors, *J. Power Sources* 228 (2013) 193–197.
- [32] C.H. Kim, J.-H. Wee, Y.A. Kim, K.S. Yang, C.-M. Yang, Tailoring pore structure of carbon nanofiber for achieving ultrahigh-energy-density supercapacitors using ionic liquid as electrolyte, *J. Mater. Chem. A* 4 (2016) 4763–4770.
- [33] S. Wu, G. Chen, N.Y. Kim, K. Ni, W. Zeng, Y. Zhao, Z. Tao, H. Ji, Z. Lee, Y. Zhu, Creating pores on graphene platelets by low-temperature KOH activation for enhanced electrochemical performance, *Small* 12 (2016) 2376–2384.
- [34] Y. Liu, J. Goebel, Y. Yin, Templated synthesis of nanostructured materials, *Chem. Soc. Rev.* 42 (2013) 2610–2653.
- [35] H. Nishihara, T. Kyotani, Templated nanocarbons for energy storage, *Adv. Mater.* 24 (2012) 4473–4498.
- [36] X. He, X. Li, H. Ma, J. Han, H. Zhang, C. Yu, N. Xiao, J. Qiu, ZnO template strategy for the synthesis of 3D interconnected graphene nanocapsules from coal tar pitch as supercapacitor electrode materials, *J. Power Sources* 340 (2017) 183–191.
- [37] W. Lin, B. Xu, L. Liu, Hierarchical porous carbon prepared by NaOH activation of nano-CaCO<sub>3</sub> templated carbon for high rate supercapacitors, *New J. Chem.* 38 (2014) 5509–5514.
- [38] H. Itoi, H. Nishihara, T. Kogure, T. Kyotani, Three-dimensionally arrayed and mutually connected 1.2-nm nanopores for high-performance electric double layer capacitor, *J. Am. Chem. Soc.* 133 (2011) 1165–1167.
- [39] W. Liang, Y. Zhang, X. Wang, Y. Wu, X. Zhou, J. Xiao, Y. Li, H. Wang, Z. Li, Asphalt-derived high surface area activated porous carbons for the effective adsorption separation of ethane and ethylene, *Chem. Eng. Sci.* 162 (2017) 192–202.
- [40] Y. Liu, P. Li, Y. Wang, J. Liu, Y. Wang, J. Zhang, M. Wu, J. Qiu, A green and template recyclable approach to prepare Fe<sub>3</sub>O<sub>4</sub>/porous carbon from petroleum asphalt for lithium-ion batteries, *J. Alloys Compd.* 695 (2017) 2612–2618.
- [41] X. He, H. Ma, J. Wang, Y. Xie, N. Xiao, J. Qiu, Porous carbon nanosheets from coal tar for high-performance Supercapacitors, *J. Power Sources* 357 (2017) 41–46.
- [42] T. Wang, R. Villegas Salvatierra, A.S. Jalilov, J. Tian, J.M. Tour, Ultrafast charging high capacity asphalt–lithium metal batteries, *ACS Nano* 11 (2017) 10761–10767.
- [43] B. Cao, H. Liu, B. Xu, Y. Lei, X. Chen, H. Song, Mesoporous soft carbon as an anode material for sodium ion batteries with superior rate and cycling performance, *J. Mater. Chem. A* 4 (2016) 6472–6478.
- [44] M. Li, C. Liu, H. Cao, H. Zhao, Y. Zhang, Z. Fan, KOH self-templating synthesis of three-dimensional hierarchical porous carbon materials for high performance supercapacitors, *J. Mater. Chem. A* 2 (2014) 14844.
- [45] D. Shan, J. Yang, W. Liu, J. Yan, Z. Fan, Biomass-derived three-dimensional honeycomb-like hierarchical structured carbon for ultrahigh energy density asymmetric supercapacitors, *J. Mater. Chem. A* 4 (2016) 13589–13602.
- [46] X. He, R. Li, J. Qiu, K. Xie, P. Ling, M. Yu, X. Zhang, M. Zheng, Synthesis of mesoporous carbons for supercapacitors from coal tar pitch by coupling microwave-assisted KOH activation with a MgO template, *Carbon* 50 (2012) 4911–4921.
- [47] R. Lin, P. Huang, J. Ségalini, C. Largeot, P.L. Taberna, J. Chmiola, Y. Gogotsi, P. Simon, Solvent effect on the ion adsorption from ionic liquid electrolyte into sub-nanometer carbon pores, *Electrochim. Acta* 54 (2009) 7025–7032.
- [48] Y. Zhu, S. Zhang, J.-J. Shan, L. Nguyen, S. Zhan, X. Gu, F. Tao, In situ surface chemistries and catalytic performances of ceria doped with palladium, platinum, and rhodium in methane partial oxidation for the production of syngas, *ACS Catal.* 3 (2013) 2627–2639.
- [49] F.F. Tao, Synthesis, catalysis, surface chemistry and structure of bimetallic nanocatalysts, *Chem. Soc. Rev.* 41 (2012) 7977–7979.
- [50] X. Wei, X. Jiang, J. Wei, S. Gao, Functional groups and pore size distribution do matter to hierarchically porous carbons as high-rate-performance supercapacitors, *Chem. Mater.* 28 (2016) 445–458.
- [51] D. Hulicova-Jurcakova, M. Seredych, G.Q. Lu, T.J. Bandosz, Combined effect of nitrogen- and oxygen-containing functional groups of microporous activated carbon on its electrochemical performance in supercapacitors, *Adv. Funct. Mater.* 19 (2009) 438–447.
- [52] T.-X. Shang, R.-Q. Ren, Y.-M. Zhu, X.-J. Jin, Oxygen- and nitrogen-co-doped activated carbon from waste particleboard for potential application in high-performance capacitance, *Electrochim. Acta* 163 (2015) 32–40.
- [53] Z.-Q. Hao, J.-P. Cao, Y. Wu, X.-Y. Zhao, Q.-Q. Zhuang, X.-Y. Wang, X.-Y. Wei, Preparation of porous carbon sphere from waste sugar solution for electric double-layer capacitor, *J. Power Sources* 361 (2017) 249–258.
- [54] B. Xu, D. Zheng, M. Jia, G. Cao, Y. Yang, Nitrogen-doped porous carbon simply prepared by pyrolyzing a nitrogen-containing organic salt for supercapacitors, *Electrochim. Acta* 98 (2013) 176–182.
- [55] J. Zhao, Y. Jiang, H. Fan, M. Liu, O. Zhuo, X. Wang, Q. Wu, L. Yang, Y. Ma, Z. Hu, Hydrophilic hierarchical nitrogen-doped carbon nanocages for ultrahigh supercapacitive performance, *Adv. Mater.* 29 (2017) 1604569.
- [56] D.-D. Zhou, W.-Y. Li, X.-L. Dong, Y.-G. Wang, C.-X. Wang, Y.-Y. Xia, A nitrogen-doped ordered mesoporous carbon nanofiber array for supercapacitors, *J. Mater. Chem. A* 1 (2013) 8488–8496.
- [57] H. An, Y. Li, P. Long, Y. Gao, C. Qin, C. Cao, Y. Feng, W. Feng, Hydrothermal preparation of fluorinated graphene hydrogel for high-performance supercapacitors, *J. Power Sources* 312 (2016) 146–155.
- [58] D.-D. Zhou, Y.-J. Du, Y.-F. Song, Y.-G. Wang, C.-X. Wang, Y.-Y. Xia, Ordered hierarchical mesoporous/microporous carbon with optimized pore structure for supercapacitors, *J. Mater. Chem. A* 1 (2013) 1192–1200.